Patterns

Article

Long-sequence voltage series forecasting for internal short circuit early detection of lithium-ion batteries

Graphical abstract

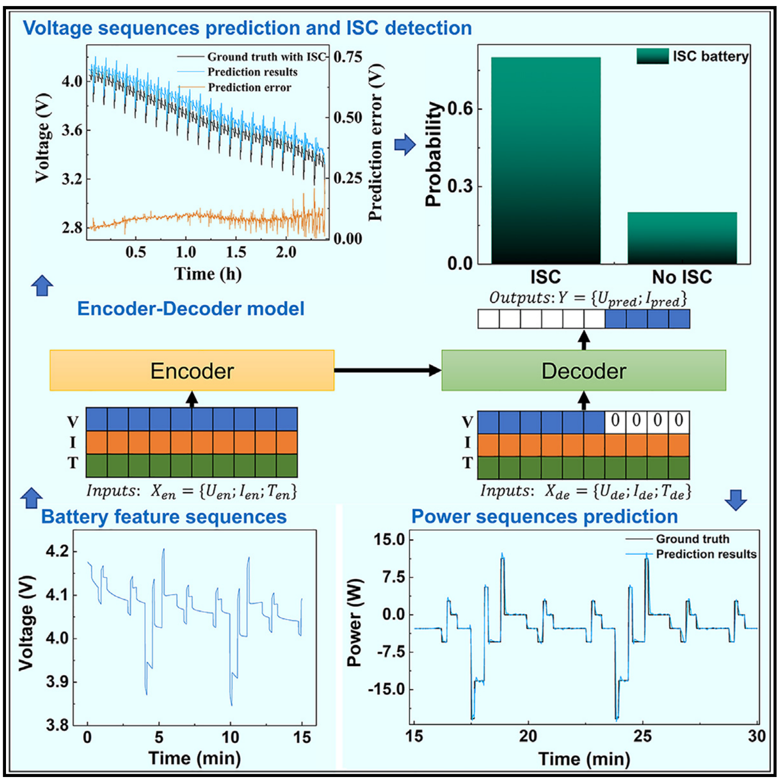

Highlights

- A deep learning method is proposed to predict future voltage and power series
- The method can accurately forecast voltage and power series over battery life
- Evolution inconsistency of normal and ISC battery voltage is used to detect ISC
- Early ISC of different types of batteries can be detected accurately and quickly

Authors

Binghan Cui, Han Wang, Renlong Li, ..., Pengjian Zuo, Guokang Han, Chunyu Du

Correspondence

gkhan@hit.edu.cn (G.H.),
cydu@hit.edu.cn (C.D.)

In brief

Cui et al. demonstrate the feasibility of deep learning methods for early detection of internal short circuits (ISCs). It provides a deep learning method based on encoder-decoder architecture for forecasting voltage and power sequences by taking the historical time series as input. Through the evolution inconsistency of normal and ISC battery voltage, it offers a new way to accurately detect early ISCs.

Cui et al., 2023, Patterns 4, 100732
June 9, 2023
https://doi.org/10.1016/j.patter.2023.100732

CellPress

Patterns

CellPress OPEN ACCESS

Article

Long-sequence voltage series forecasting for internal short circuit early detection of lithium-ion batteries

Binghan Cui,[1] Han Wang,[1] Renlong Li,[1] Lizhi Xiang,[1] Jiannan Du,[1] Huaian Zhao,[1] Sai Li,[1] Xinyue Zhao,[1] Geping Yin,[1] Xinqun Cheng,[1] Yulin Ma,[1] Hua Huo,[1] Pengjian Zuo,[1] Guokang Han,[1,*] and Chunyu Du[1,2,*]

[1]MIIT Key Laboratory of Critical Materials Technology for New Energy Conversion and Storage, School of Chemistry and Chemical Engineering, Harbin Institute of Technology, Harbin 150001, China

[2]Lead contact

*Correspondence: gkhan@hit.edu.cn (G.H.), cydu@hit.edu.cn (C.D.)

https://doi.org/10.1016/j.patter.2023.100732

THE BIGGER PICTURE Lithium-ion batteries are applied in many fields because of their high energy and power density. However, accidents associated with battery fires have raised great public awareness and concerns about safety issues. Internal short circuits (ISCs) are the main reason for battery fires. However, so far, there is still a lack of accurate and quick methods for ISC detection. To address this challenge, we report a method to predict future battery characteristics using deep learning. ISCs can be detected accurately and quickly by inconsistency of the evolution of normal and ISC battery characteristics. The method is demonstrated over the full life cycle of batteries. The general method can also be applied to fault detection of many other mechanical and electronic systems. The long-term goal of this research is to achieve a digital twin with broader applications for intelligent battery management, such as prolonging battery life and optimizing charging profiles.

1 2 3 4 5 **Proof-of-Concept:** Data science output has been formulated, implemented, and tested for one domain/problem

SUMMARY

Accurate early detection of internal short circuits (ISCs) is indispensable for safe and reliable application of lithium-ion batteries (LiBs). However, the major challenge is finding a reliable standard to judge whether the battery suffers from ISCs. In this work, a deep learning approach with multi-head attention and a multi-scale hierarchical learning mechanism based on encoder-decoder architecture is developed to accurately forecast voltage and power series. By using the predicted voltage without ISCs as the standard and detecting the consistency of the collected and predicted voltage series, we develop a method to detect ISCs quickly and accurately. In this way, we achieve an average percentage accuracy of 86% on the dataset, including different batteries and the equivalent ISC resistance from 1,000 Ω to 10 Ω, indicating successful application of the ISC detection method.

INTRODUCTION

Lithium-ion batteries (LiBs) enable a wide range of applications because of their high energy density and long cycle life.[1–5] However, frequent accidents associated with thermal runaway (TR) have raised concerns about the safety of LiBs.[6–9] Localized hotspots triggered by an internal short circuit (ISC) that propagate throughout the cell are believed to be one of the main reasons for TRs.[10–12] Therefore, accurate early detection of ISCs is of great significance for informing the user of safety risks and judging whether LiBs are in healthy condition, which contributes to safer utilization of LiBs and improvement of the equipment's overall safety level.[13,14]

Many ISC detection methods have been proposed and are generally classified into threshold-based and model-based methods. ISCs are often accompanied by abnormal behavior in parameters with a fixed variation range over the full life cycle. Therefore, as long as parameters such as deviation, correlation coefficient, and entropy of voltage,[15–20] temperature,[18] and impedance[19,20] exceed the threshold set in advance, ISCs can be detected. Threshold-based methods do not need complex battery models or algorithms and can be easily implemented in battery management systems (BMSs). However, the challenge of threshold-based methods is to set proper thresholds under different working conditions and life cycles because of the dynamic characteristics of the battery. Model-based methods detect ISCs by model parameters and estimated states such as changes in voltage,[21] state of charge (SOC),[21–25] and capacity.[26] The residuals can be obtained by comparing the measurable parameter or state with the parameters or states generated by the model, which are then utilized for evaluating ISCs. Generally, model-based methods that simulate the charging and discharging characteristics of the battery are more accurate than threshold-based methods. However, the ISC detection accuracy of the model-based methods is highly dependent on the simulation accuracy of the models. Constructing a model that can accurately simulate the behavior of LiBs under different operational conditions is still challenging because of the difficulties in modeling many degradation modes and their coupling with thermal and other fields within the battery.

Conventional model-based methods utilize voltage-based and physically based models to simulate LiBs, thereby diagnosing the ISCs. Recently, because of advances in computational power, using deep learning methods to model LiBs and predict their charging and discharging behavior has become attractive. Such methods do not require accurate battery models but establish an accurate mapping between inputs and outputs, which can help us omit the complex battery modeling process. The voltage evolution for normal and ISC batteries is inconsistent under the condition of the same collected current. When an ISC occurs, part of the collected current is used for the ISC, and the rest is used for charging and discharging, which leads to a deviation between the collected and actual current induced by the ISC, but this is the same as in normal LiBs.[27] Therefore, learning the evolution of normal battery voltage offline by deep learning methods, implementing a digital twin of batteries, forecasting long-sequence voltage series online by history voltage, and detecting battery faults based on the inconsistent voltage evolution of normal and ISC battery voltages is no doubt an efficient method. Hong et al.[28] predicted voltage in the next second based on a long short-term memory (LSTM) recurrent neural network and an equivalent circuit model to achieve potential failure risk assessment and issue an early TR warning accordingly. Liu et al.[29] constructed a physical model to simulate an ISC battery, extracted features from the physical model, and utilized LSTM to detect ISCs. Cao et al.[30] built a diagram of the adaptive integrated prediction algorithm combining a mean-difference model and a bidirectional LSTM to predict voltage, detecting ISCs and TRs. Voltage change caused by leakage current is insignificant, making early detection of ISCs challenging. Generally, it takes several minutes to produce a significant voltage change[20] for early ISCs where the equivalent ISC resistance is greater than 100 Ω (Figure S1). Hence, a model that can accurately forecast long-sequence voltage series is required for early detection of ISCs. In addition, because of peak and frequency regulation requirements for smart grids[31] and highly accurate calculation of remaining mileage[32] or energy[33] for electric vehicles, long sequence power series forecasting has become another challenge.

In this work, we develop deep learning methods based on encoder-decoder architecture that can accurately forecast the long-sequence voltage and power series of commercial $LiNi_{0.5}Co_{0.2}Mn_{0.3}O_2$/graphite (NCM523) and $LiNi_{0.8}Co_{0.1}Mn_{0.1}O_2$/graphite (NCM811) batteries. The developed methods utilize a multi-head attention mechanism, residual connections, and hierarchical learning mechanism, which can more accurately learn the voltage evolution better and construct the mapping between the historical voltage or power series and voltage or power series in the future. Because of the inconsistency of the collected current and real current of the ISC battery and the dynamic characteristics of the leakage current (when the equivalent ISC resistance is constant), there is a larger voltage series prediction error for an ISC battery than for a normal battery. We develop a method for ISC detection that can bridge voltage predictions with triggering of ISCs. This method uses the difference in voltage prediction error between normal and ISC batteries as the judgment criteria of ISCs. We generated a dataset including 62 NCM811 and 8 NCM523 batteries under different constant current (CC), dynamic stress test (DST), and random test (RT) discharge conditions with equivalent ISC resistance ranging from 1,000 Ω to 10 Ω to train and validate the performance of the proposed method. By adjusting the input length, our methods can flexibly forecast voltage and power series with different lengths. In the scenario of predicting the voltage series in the next 8 min based on the 8-min historical voltage series, we can achieve prediction errors under CC, DST, and RT conditions of 11.7, 19.3, and 9.8 mV (0.3%, 0.5%, and 0.3% of the nominal voltage of 3.7 V, respectively) and 19.5 mV over the full cycle of NCM811 batteries. We can also achieve prediction errors under CC and DST conditions of 10 and 33.3 mV, respectively, for NCM523 batteries. In the scenario of forecasting the power series in the next 8 min based on the 8-min historical power series, we can achieve prediction errors under DST and RT conditions of 0.7 and 0.15 W (3.4% and 0.7% of the maximum discharge power of 20.8 W, respectively) and 1.6 W over the full life cycle of NCM811 batteries. Furthermore, using the predicted voltage series, we achieve a micro-ISC detection accuracy of 86% under 49 different working conditions, 85% over the full life cycle of NCM811 batteries, and 81% under 8 different working conditions of NCM523 batteries through deep learning methods. These results demonstrate the power of the method to accurately detect ISCs in different working conditions, battery types, and life cycles. Our methods can also be applied to problems such as TRs, lithium precipitation, and external short circuits, which can lead to abnormal voltage behavior,[1,34–36] and our methods can achieve early detection and warning.

RESULTS

Data generation

In this study, commercial NCM811 and NCM523 batteries were cycled in a temperature-controlled environment (25°C) under various charging-discharging conditions with voltage windows ranging from 2.75–4.2 V (Table S1). The specifications of the battery are listed in Table S2. Batteries 1–36 are cycled under CC working conditions, batteries 37–56 are cycled under DST working conditions, and battery 57 is cycled under RT working

Table 1. Model metrics for the normal battery voltage prediction results under different working operations and battery types in the case of forecasting the voltage series in the next 8 min based on the historical 8-min time series

Metrics (mV)	Battery types/working conditions					
	NCM811/CC	NCM811/DST	NCM811/RT	NCM523/CC	NCM523/DST	NCM811/FL
MAE	11.7	19.3	9.8	9.9	30.7	19.6
RMSE	17.7	34.4	13.5	15.9	49.5	23.2

CC, DST, and RT refer to the working operations listed in Table S1. FL refers to the normal tests over the full life cycle of battery 58.

conditions. Each discharge rate under RT working conditions obeys a uniform distribution with a maximum discharge rate of 2 C; the detailed working operations are listed in Table S3. The RT working conditions simulate real working conditions and validate our proposed methods. Batteries 58–70 are conducted for approximately 400 cycles with capacities down to 77% of the initial capacity. Battery 58 is cycled under the normal test, and batteries 59–70 are cycled under the ISC test. The equivalent ISC resistances paralleled to batteries 59–70 are listed in Table S4. Batteries 1–57 are used for 28 cycles (Table S5), in which normal and ISC tests are processed alternately. In the ISC test, the equivalent ISC resistance from 1,000 to 10 Ω is parallel to the battery to simulate ISCs of different severities.[37] Detailed loading profiles of the batteries can be found in Note S1. The discharge voltage curves of batteries show a declining trend with increasing cycle numbers and decreasing equivalent ISC resistance, as presented in Figures S2–S5. The capacity degradation of batteries 58–70 is shown in Figure S6. Then, a window of length 2 m is used to scan the entire time series to obtain samples containing outputs, encoder inputs, and decoder inputs (Figure S7). The decoder inputs contain the second half of the encoder inputs and a 0 sequence of length m. The encoder and decoder inputs include time, current, and voltage series. The output only contains voltage series in the voltage prediction scenario but involves voltage and current series in the power prediction scenario. The voltage or power prediction dataset we generated contains approximately 3 million samples, which can systematically validate the proposed method. Finally, the samples generated by each cycle with the normal test are randomly divided into prediction training, validation, and test sets at a ratio of 7:2:1. The input of the ISC detection method is the concatenation of the voltage prediction results and output of the samples generated by each cycle with the normal test and ISC test. The target values of the inputs generated by the ISC test and the normal test are set to 1 and 0, respectively. The inputs and targets are divided into detection training and validation sets.

Long-sequence voltage series forecasting

Based on the historical time, current, and voltage series, a deep learning method based on encoder-decoder architecture[38–40] (see Experimental procedures for detailed information on our proposed method) is used to forecast the long-sequence voltage. Standard feature normalization is performed on the prediction training set to obtain the same distribution. The features of the prediction validation and test sets are normalized by applying the same normalizing scales as used on the prediction training set. Two metrics, defined under Deep learning method development section, are used to evaluate our predictive performance, mean absolute error (MAE) and root-mean-square error (RMSE), with units of millivolts, amperes, and watts in the voltage, current, and power prediction scenarios, respectively.

We evaluate our proposed methods through five different input/output sequence lengths and working conditions. In the case of the same input sequence length, the prediction performance decreases as the output sequence length increases, as presented in Table S6. The reason for the decline in prediction performance is that, with the increase in prediction length and uncertainty of the output, obtaining high-confidence results and establishing an accurate mapping between the output and input is difficult. Over the entire SOC range of batteries, the proposed method can predict the 8-min voltage sequences with MAEs of 11.7, 19.3, and 9.8 mV (0.3%, 0.5%, and 0.3% of the nominal voltage of 3.7 V, respectively) under CC, DST, and RT working conditions of NCM811 batteries, as presented in Table 1. The proposed method can also predict the 8-min voltage sequences with MAEs of 9.9 and 30.7 mV (0.3% and 0.8% of the nominal voltage of 3.7 V, respectively) under CC and DST working conditions of NCM523 batteries, which indicates that the proposed method can maintain strong robustness and accuracy for different types of batteries. Finally, we demonstrate that the proposed method can achieve highly accurate forecasting performance with an MAE of 19.6 mV (0.5% of the nominal voltage of 3.7 V) over the full life cycle of the NCM811 battery. We randomly select the prediction results of batteries 33 and 1 to show the performance of our proposed method. The voltage prediction examples of the NCM811 and NCM523 batteries under DST, CC, and RT working conditions are plotted in Figure S8. It can be seen that the accuracy of the proposed method worsens at the end of the discharge process under both working conditions, which is due to the rapid change in voltage caused by battery polarization at the end of the discharge process. The 8-min voltage prediction results are shown in Figures 1A–1F and S9–S11 as a function of the predicted length and the starting voltage of the input sequence. It can be seen that the proposed method has the best prediction performance when the starting voltage is larger than 3.4 V and the predicted length is less than 300, as indicated by the deep color. We also demonstrate that the proposed method can achieve accurate prediction even under RT working conditions and over the full life cycle of the battery. The distribution of the voltage prediction error is plotted in Figure 1G. The prediction performance of our proposed method is not sensitive to the working conditions, and our proposed method can achieve accurate and robust prediction results in daily applications. To further demonstrate the performance of our proposed method, we adopt four widely used deep learning techniques as baseline methods: convolutional neural network (CNN), deep neural network (DNN), gate

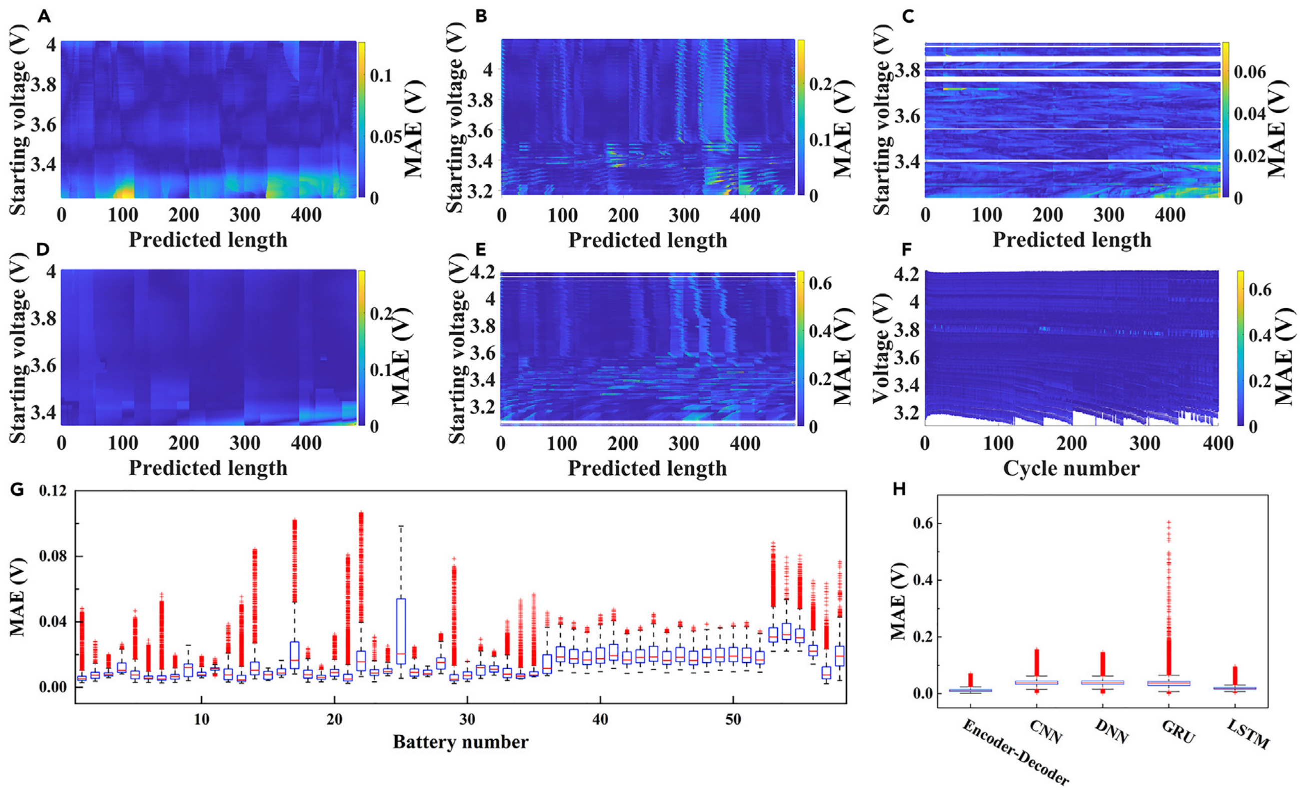

Figure 1. Normal test battery voltage prediction results with the output of 8-min voltage sequences

(A–F) MAE of voltage prediction for battery 1 (A), battery 37 (B), battery 57 (C), battery 33 (D), battery 53 (E), and battery 58 (F). In (A)–(E), the x axis is the predicted length of the voltage prediction results, and the y axis is the starting voltage of the input sequence. In (F), the x axis is the cycle number, and the y axis is the discharge voltage. The color indicates the MAE.

(G) Error distribution of the voltage prediction results of batteries 1–58.

(H) Error distribution of the voltage prediction results of batteries 1–58. CNN, DNN, GRU, and LSTM are adopted as baseline methods.

recurrent unit neural network (GRU), and LSTM. Each method uses the same input data as our proposed method. The distribution of their estimation errors is plotted in Figure 1H, and the MAE and RMSE of these methods are listed in Table S7. It can be seen that our proposed method has high accuracy with the smallest prediction error and error distribution. The CNN, DNN, and GRU fail to provide reliable voltage prediction sequences with MAE and RMSE over 30 mV. In contrast, the LSTM has better performance, but the MAE, RMSE, and error distribution are still worse than those of our proposed methods. A detailed description and comparison of the computing efficiency and performance of the four baseline methods and our proposed methods can be found in Note S2. In this region, the proposed method can predict reliable voltage sequence results, which can prevent overcharge and overdischarge, give a notification about the remaining operating time, monitor the state, and diagnose degradation.[41–47]

Long-sequence power series forecasting

The results in Figure 1 demonstrate that we can accurately predict voltage sequences as a function of the historical time series. Moreover, the voltage and current sequences can be predicted simultaneously, enabling prediction of the corresponding power sequences by using $P = U \times I$, where P, U, and I are the power, voltage, and current prediction results, respectively. In the power prediction scenario, considering that the current of CC working conditions is constant, we only use data from DST working conditions to evaluate our proposed method. The power prediction results and errors for the entire voltage range and 8 min are shown in Figure S12 and Table S9. It is shown that the prediction error increases with the output sequence length. Table 2 and Figures 2A–2D and S13 display the performance of our proposed methods applied to the different working conditions. The proposed method can predict the 8-min sequences of power of the NCM811 battery with an MAE of 0.7 W (4.2% of the maximum discharge power of 20.8 W) under DST working conditions and 0.2 W (1.0% of the maximum discharge power of 20.8 W) under RT working conditions. Then, the data from the NCM523 battery are used to validate the accuracy and robustness of the proposed method. The MAE is 1.5 W under DST working conditions in the case of predicting the 8-min power sequences of the NCM523 battery, which is twice the MAE of the NCM811 battery. The reason for the larger error of the NCM523 battery is that the size of the NCM811 battery dataset is larger than that of the NCM523 battery dataset, so the proposed method can learn the power evolution of the NCM811 battery better than that of the NCM523 battery. The proposed method can also achieve accurate performance over the full

Table 2. Model metrics for the normal battery power prediction results under different working operations and battery types in the case of forecasting the power series in the next 8 min based on the historical 8-min time series

Metrics (W)	Battery types/working conditions			
	NCM811/DST	NCM811/RT	NCM523/DST	NCM811/FL
MAE	0.7	0.2	1.5	1.6
RMSE	1.7	0.2	2.3	3.1

DST and RT refer to the different working operations listed in Table S1. FL refers to the normal tests over the full life cycle of battery 58.

life cycle of the NCM811 battery with an MAE of 1.6 W. The proposed method's performance in predicting the 8-min power sequence of the NCM811 battery is benchmarked against four widely used deep learning methods: CNN, DNN, GRU, and LSTM. The error distribution, MAE, and RMSE of these methods are shown in Figure 2F and Table S10. The CNN, DNN, and GRU achieve worse performance with their MAE and RMSE over 2 W. In contrast, LSTM has better performance, but the MAE, RMSE, and error distribution are still worse than our proposed methods. Similar to voltage prediction, when the historical voltage and current sequences are known, the power sequences in the future can be predicted accurately, which is beneficial for peak and frequency regulation of smart grids[31] and the calculation of remaining mileage or energy calculation of electric vehicles.[32,33]

ISC detection

As mentioned earlier, the collected current and real current are inconsistent when the battery suffers from ISCs, which will cause inconsistency between normal and ISC battery voltage evolution.[27] Therefore, based on such inconsistency, accurate voltage sequence prediction makes our proposed method capable of detecting ISCs. We use the historical time series from the ISC test to predict the ISC test voltage sequences. Examples of discharge voltage prediction results with an equivalent ISC resistance of 10 Ω are shown in Figures 3A–3C, S14A, and S14B. The results reveal that, after our proposed method learns the voltage evolution from normal batteries, regardless of the working conditions, there will be a larger error in predicting the voltage sequences of the ISC test compared with the normal test because of the leakage current. The distribution of the voltage prediction error and the equivalent ISC resistance from 1,000 Ω to 10 Ω and MAE of voltage prediction results are plotted in Figures 3D–3I and S14. The MAE of battery 37 reaches the minimum and maximum under the equivalent ISC resistance of 100 Ω and 10 Ω, which are 2.2 and 5.0 times the normal test MAE of 8.3 mV, respectively; this phenomenon can also be found under CC and RT working conditions as well as in NCM523 batteries. It can also be seen that the MAE shows an increasing trend with ISC severity, which is beneficial for ISC detection.

The voltage prediction errors of the ISC test for different working conditions and battery types are plotted in Figures 4 and S15–S20. It also shows that the MAE increase is caused by the equivalent ISC resistance. The working conditions play a critical role in battery performance because the change in working conditions will always greatly influence degradation.[48] It is demonstrated that the phenomenon where the MAE of voltage predictions of the ISC test is larger than that of the normal test is common under different operating conditions and battery

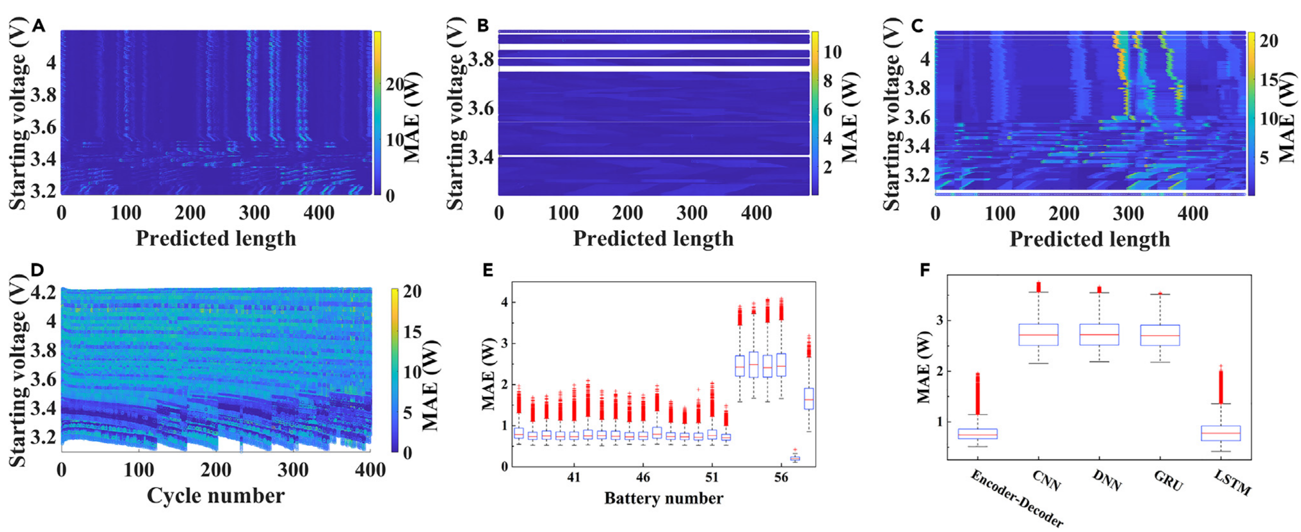

Figure 2. Normal test battery power prediction results with the output of 8-min voltage and current sequences

(A–D) MAE of power prediction results for battery 37 (A), battery 57 (B), battery 53 (C), and battery 58 (D). In (A)–(C), the x axis is the predicted length of the prediction results, and the y axis is the starting voltage of the input sequence. In (D), the x axis is the cycle number, and the y axis is the discharge voltage. The color indicates the MAE.

(E) Error distribution of the power prediction results.

(F) Error distribution of the power prediction results. CNN, DNN, GRU, and LSTM are adopted as baseline methods.

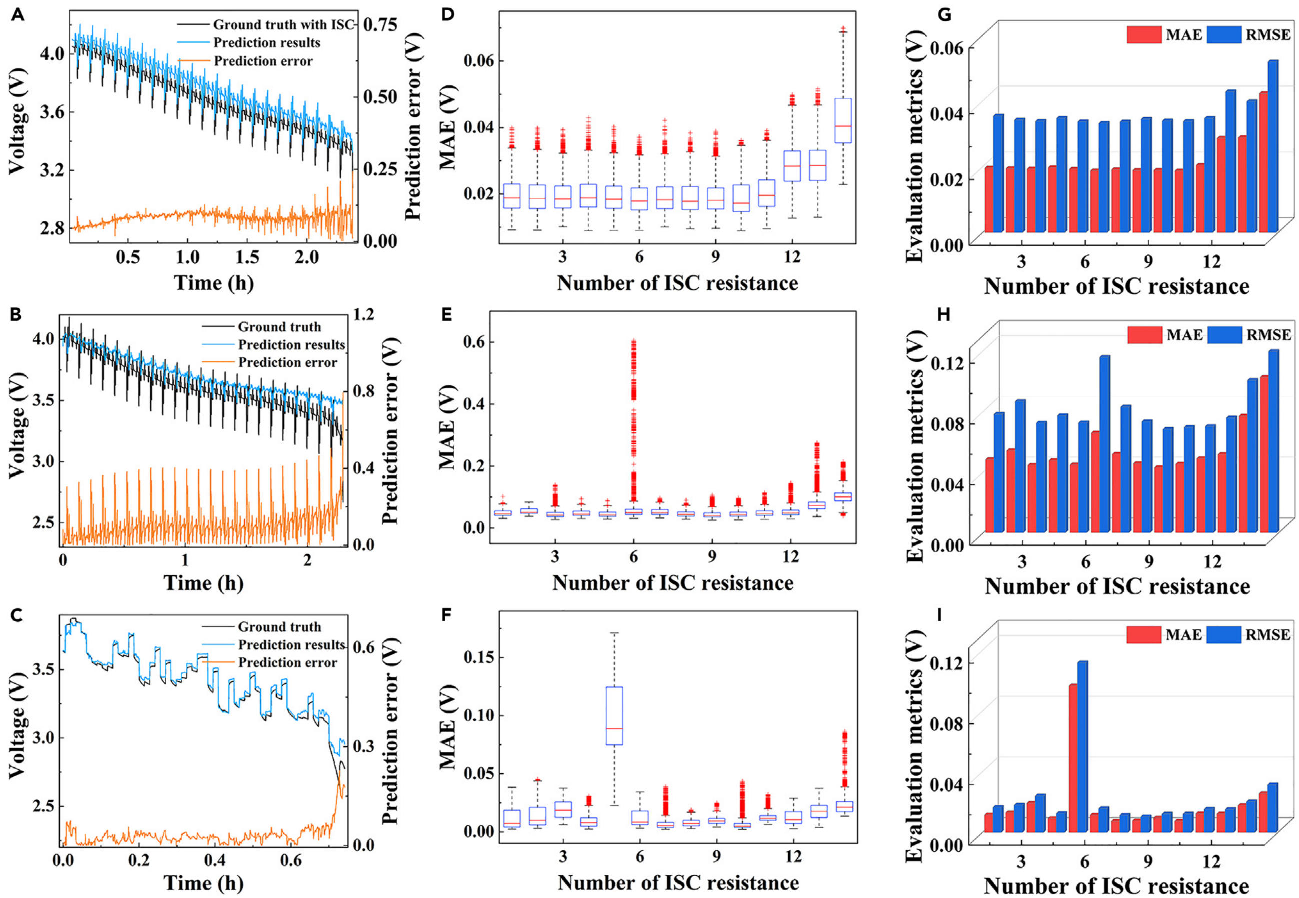

Figure 3. Battery voltage prediction results of the ISC test with the output of 8-min voltage sequences
(A–C) Examples of voltage prediction results for battery 37 (A), battery 53 (B), and battery 57 (C) with an equivalent ISC resistance of 10 Ω.
(D–F) Error distribution of the prediction results with the equivalent ISC resistance from 1,000 Ω to 10 Ω for battery 37 (D), battery 53 (E), and battery 57 (F).
(G–I) Voltage prediction MAE and RMSE of the ISC test for battery 37 (G), battery 53 (H), and battery 57 (I).
In (D)–(I), the x axis is the amount of equivalent ISC resistance, where 1–14 correspond to the equivalent ISC resistance of 1,000 Ω–10 Ω, respectively.

types. It also shows that the MAE is sensitive to the equivalent ISC resistance but not sensitive to the working conditions, demonstrating the strong robustness of our proposed method.

Figures 3 and 4 show that we can detect the evolution inconsistency of the voltage sequences between the normal and ISC tests. Based on the inconsistency, we developed a detection method (Figure 6B) to diagnose ISCs. We generate detection training and validation sets of different equivalent ISC resistances. The detection training sets are used to set the model weights, and the detection validation sets are used to evaluate the method's performance. The proposed ISC detection method yields the probability of ISCs, and the battery will be classified into the ISC group when the probability is larger than 0.5. Average percentage accuracy, defined under Deep learning method development, is used to evaluate the ISC detection performance.

Table S11 and Figure 5A display the performance of our proposed ISC detection method applied to our datasets of the NCM811 battery. With the output of the 2-min voltage sequences, we achieve approximately 87% average percentage accuracy on the detection validation sets, including the equivalent ISC resistance from 50 Ω to 10 Ω, which always needs several hours to detect through conventional methods. However, poor performance was obtained on the datasets containing the equivalent ISC resistance from 1,000 Ω to 100 Ω with a 64% average percentage accuracy. The reason for achieving more accurate ISC detection when the equivalent resistance of ISCs is small is that, with the increase in the equivalent resistance of ISCs, the MAE between the predicted voltage sequence and the collected voltage sequence will gradually decrease, making ISC detection difficult. We select inputs with a longer voltage sequence to detect ISCs, considering that the changes in battery voltage caused by leakage current always require a long time to be detected.[20] As expected, by increasing the length of the voltage sequences, the average percentage error of the detection validation sets, including the equivalent ISC resistance from 1,000 Ω to 100 Ω, decreases to 14%, which proves the accuracy and robustness of our proposed ISC detection method. The reason why we discuss voltage, power forecasting, and ISC detection in different periods is to apply our methods better in different scenarios. If only ISCs with 100 Ω need to be detected, predicting 120-s voltage sequences can be a good

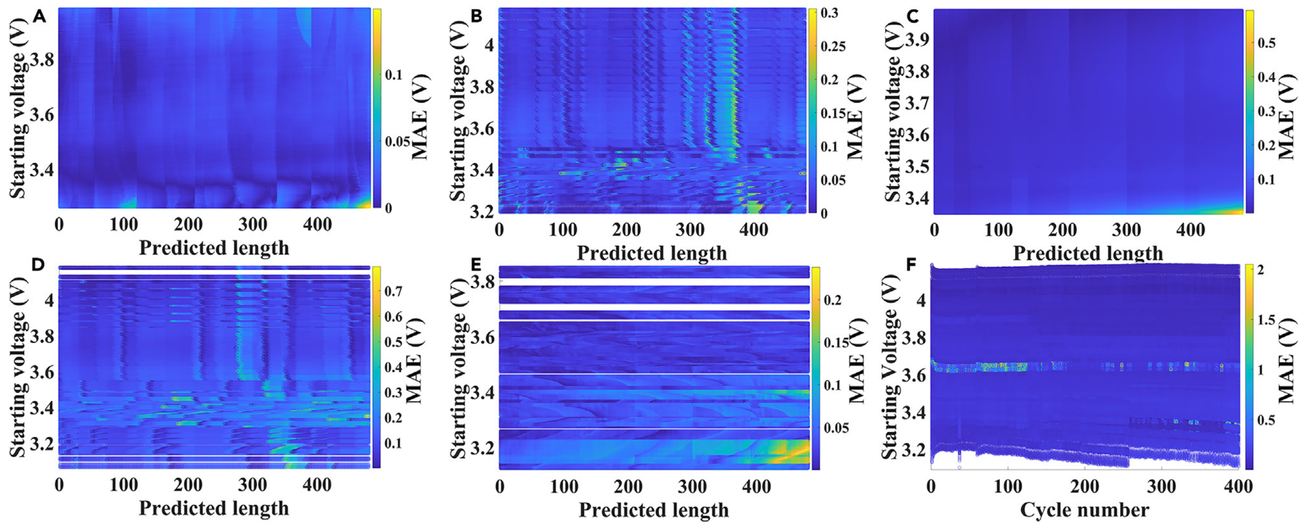

Figure 4. Battery voltage prediction error of the ISC test with the output of 8-min voltage sequences

(A–F) MAE of voltage prediction results for battery 1 (A), battery 37 (B), battery 33 (C), battery 53 (D), battery 57 (E), and battery 59 (F) with the equivalent ISC resistance of 10 Ω. In (A)–(E), the x axis is the predicted length of the prediction results, and the y axis is the starting voltage of the input sequence. In (F), the x axis is the cycle number, and the y axis is the discharge voltage. The color indicates the MAE.

solution, reducing unnecessary memory consumption and improving computing efficiency. Table S12 and Figure 5B display the ISC detection performance of the NCM523 battery, the dataset of the NCM811 battery under RT working conditions, and the dataset over the full life cycle of the NCM811 battery. With the output of the 8-min voltage sequences, we achieve approximately 81% average percentage accuracy on the dataset of the NCM523 battery and 80% average percentage accuracy on the dataset of the NCM811 battery under RT working conditions, including the equivalent ISC resistance from 1,000 Ω to 10 Ω. We also demonstrate that the proposed methods can achieve accurate ISC early detection over the full life cycle of the NCM811 battery with 85% average percentage accuracy, including the equivalent ISC resistance from 800 Ω to 10 Ω. The performance of the proposed method is benchmarked against four widely used deep learning methods, including CNN, DNN, GRU, and LSTM. These methods used the same input as the proposed method. The detection accuracy of these methods is shown in Figure 5C and Table S13. The average ISC detection accuracy, including the equivalent ISC resistance from 1,000 Ω to 10 Ω, of the four methods is approximately 61%, which is nearly 25% lower than that of the proposed method, indicating the accuracy of the proposed method.

Finally, we conduct a comparative study around the existing methods from the size of historical data required for ISC detection and the accuracy of ISC detection. The performance of the current methods is shown in Table 3. The detection accuracy of these methods is poor when the equivalent ISC resistance is

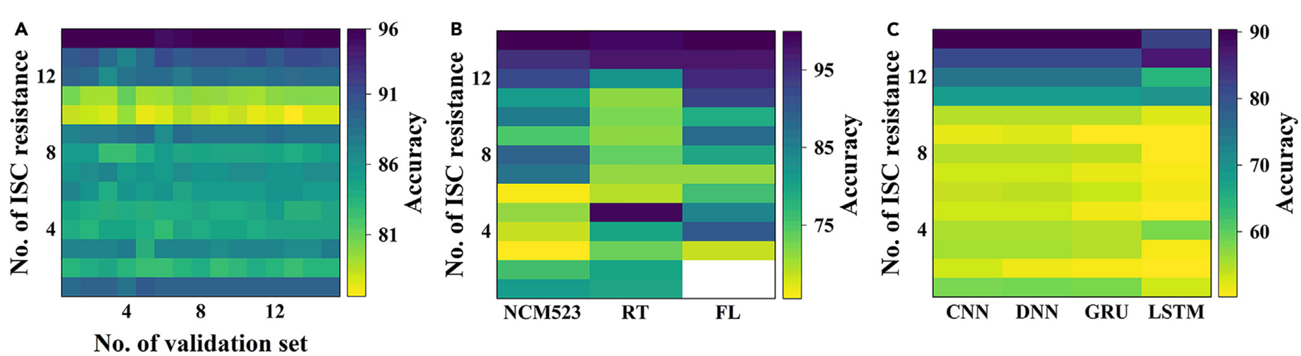

Figure 5. Accuracy of ISC detection with an input sequence length of 480

(A) ISC detection accuracy of detection validation sets of batteries 1–32 and 37–52 under various ISC equivalent resistance. The x axis is the number of detection validation sets, where 1–15 correspond to the battery number of the detection validation sets (Table S1), and the y axis is the number of equivalent ISC resistance, where 1–14 correspond to the equivalent ISC resistance of 1,000 Ω–10 Ω. The color indicates the percentage accuracy.

(B) The average ISC detection accuracy of batteries 33–36 and 53–70 under various equivalent ISC resistance.

(C) The average ISC detection accuracy of four baseline methods under various equivalent ISC resistance. CNN, DNN, GRU, and LSTM are adopted as baseline methods.

In (B) and (C), the x axis is the amount of equivalent ISC resistance, where 1–14 correspond to the equivalent ISC resistance of 1,000 Ω to 10 Ω.

Table 3. A summary of the typical ISC detection methods

Methods	ISC detection accuracy	Size of historical data
Model-based methods[13]	100% detection accuracy for ISC resistance of less than 200 Ω and 64.8% detection accuracy for ISC resistance from 1,000 Ω to 10 Ω	one cycle
Model-based methods[14]	100% detection accuracy in normal battery and 98.45% detection accuracy in faulty battery	fully discharging curve (end of discharge SOC = 5%)
Threshold-based methods[20]	100% detection accuracy for ISC resistance of 1 Ω, 10 Ω, and 100 Ω	22 min for ISC resistance of 1 Ω, 1 h 17 min for ISC resistance of 10 Ω, and 4 h 43 min for ISC resistance of 100 Ω
Model-based methods[22]	79.3% detection accuracy for ISC resistance of 50 Ω	not reported
Threshold-based methods[23]	100% detection accuracy for ISC resistance of 1 Ω and 100 Ω	2.8 h for ISC resistance of 1 Ω and 20.4 h for ISC resistance of 100 Ω
Model-based methods[49]	93.5% detection accuracy for ISC resistance of less than 100 Ω	fully charging curve (3.45 V–4.20 V)
Model-based methods[50]	94% detection accuracy for ISC resistance of less than 50 Ω	not reported
Model-based methods[51]	96.08% detection accuracy for ISC resistance of 25 Ω and 93.7% detection accuracy for ISC resistance of 10 Ω	not reported

larger than 200 Ω. These methods always need data from almost one cycle to detect ISCs, which takes a long time and may bring security risks. The proposed method can detect ISCs using only 8-min voltage sequences with 86% average accuracy to shorten the detection time, improve detection efficiency, and avoid safety risks, indicating state-of-the-art performance.

DISCUSSION

In this study, we develop a deep learning method based on encoder-decoder architecture to predict long-sequence voltage and power series. The proposed method uses historical voltage, current, and time series generated from commercial NCM811 and NCM523 batteries cycled under different working conditions as inputs. Our proposed method uses multi-head attention and a hierarchical learning mechanism to achieve higher forecasting and detection accuracy than LSTM. We demonstrate that the proposed method can accurately predict the next 8-min voltage sequences and power sequences over the full life cycle of the battery under different working conditions, which is beneficial for peak and frequency regulation of smart grids and calculation of remaining mileage or energy calculation of electric vehicles. Based on the inconsistency of normal and ISC battery voltage evolution, we propose a deep learning method to detect the probability of ISCs. We achieve an average percentage accuracy of 86% on the dataset, including different battery types and the equivalent ISC resistance from 1,000 Ω to 10 Ω using 8-min voltage sequences, which is nearly 25% higher than LSTM and other baseline methods.

The performance of forecasting the voltage, current, and power sequences comes from the architecture of the proposed method. The main work of voltage or other sequence prediction based on the deep learning method is building a mapping of the historical sequences to the future sequences. The mapping is always different when the battery is under different working conditions and aging states. It is necessary to design a unique model architecture to build accurate and robust mapping under different working conditions and over the full life cycle of the batteries. The proposed method, including positional encoding, multi-head attention mechanism, residual connections, and multi-scale hierarchical learning mechanism, can achieve more accurate voltage or other sequence predictions under different working conditions and aging states. In the input time series, the voltage of the next position is changed based on the voltage of the previous position. However, the deep learning method does not know. Here, positional encoding is proposed to add positional information to the inputs. In this way, the deep learning method can learn the spatiotemporal characteristics of inputs and achieve better performance in the time series predictions. When LSTM calculates the correlation between two positions corresponding to voltage or additional data, the initial correlation must go through all hidden layers between the two positions, which is also the same in GRU. After calculating the weights, bias, and activation functions, we can obtain the final correlation. Moreover, the farther apart the two positions are, the longer the length of the prediction sequence and the more difficult it is to establish an accurate correlation, which results in a decrease in prediction accuracy. Our proposed method uses the multi-head attention mechanism to overcome this problem. The multi-head attention mechanism can calculate the correlation between any two positions corresponding to voltage or additional data by converting the calculation of the correlation into the multiplication of the input sequences. It does not require the hidden layers to pass, and the correlation is computed independently of the distance between the two positions. Therefore, compared with LSTM, the multi-head attention mechanism can establish a more accurate mapping between the historical and prediction sequences under different working conditions and

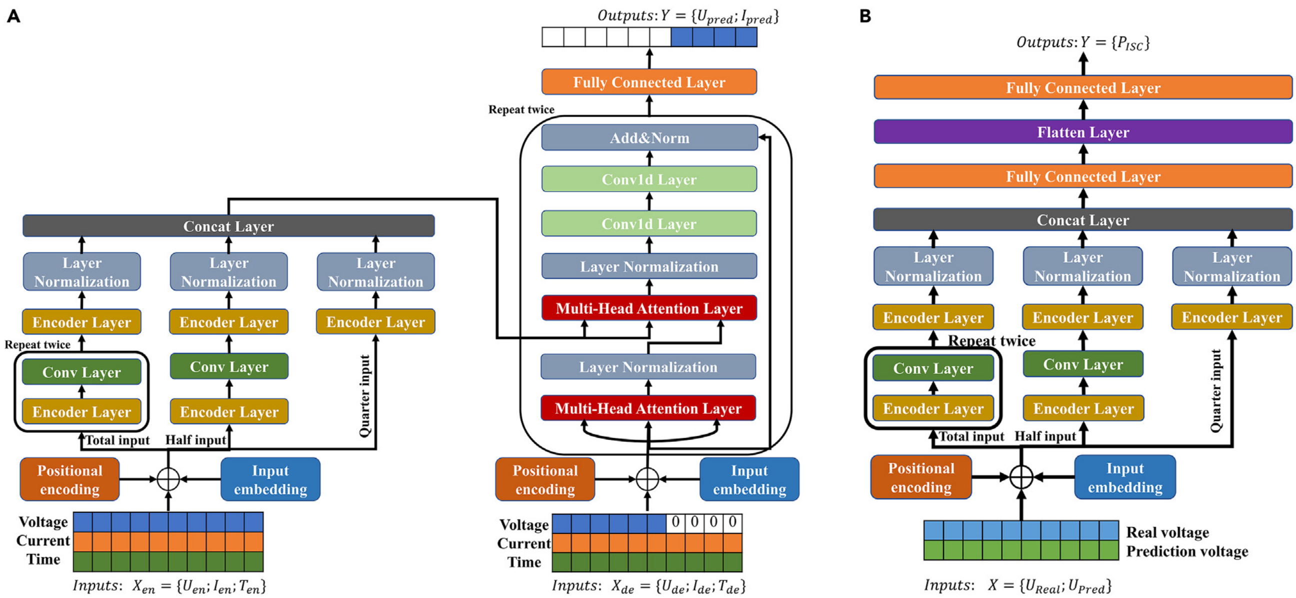

Figure 6. The architecture of the proposed model
(A) The architecture of the developed voltage and power prediction model.
(B) The architecture of the developed ISC detection model.

aging states. In addition to its higher accuracy than other methods, the multi-head attention mechanism has another advantage in terms of fast computing speed, reflecting its foresight. The model based on the multi-head attention mechanism can perform parallel computation and significantly shorten the prediction time, which is the main obstacle of the common method for time series forecasting, such as recurrent neural network (RNN). Therefore, in the face of large-scale data operation in the future, the attention model with advantages in computing speed and accuracy will slowly replace the RNN represented by LSTM and have broader application in ISC detection.

Information loss easily occurs in the calculation, resulting in prediction error. Residual connections are proposed to enter original features and extracted features together to the next calculation unit to avoid it. Moreover, we employ a multi-scale hierarchical learning mechanism. We divide the input historical time series into three groups: all historical time series, the second half of the historical time series, and the last quarter. In this way, our proposed method can learn the evolution of the overall historical time series from the first part and determine the value of the recent historical time series from the last two parts. Learning historical time series from multiple scales can reduce the difficulty of forecasting tasks and avoid the decrease in prediction accuracy because of recent historical sequence mutations. Considering the dynamic evolution of working conditions, the proposed method can also learn online. When the evolution of the current working condition is not included in the generated dataset, the proposed method can automatically update the model parameters by collecting the voltage and current to achieve accurate and robust prediction under the current working condition.

The reason why our proposed method can detect ISCs accurately lies in the features we employ. The normal battery voltage under real-life working conditions is unknown, so conventional methods always use features including normal and ISC battery information as the standard values, such as the average of normal and ISC battery voltages. The difference between the standard features and features of an ISC battery is smaller than that between the features of a normal battery and an ISC battery. Therefore, compared with using the features from the normal battery, these standard values will cause detection errors in ISC detection, regardless of whether the method is working with a normal or ISC battery. Meanwhile, the larger the equivalent ISC resistance, the longer the sequences the conventional methods need, and the poorer the ISC detection accuracy. We predict the voltage of the normal battery under current working conditions through the voltage prediction method. Then, we use the predicted voltage as the standard value and take the prediction and collection voltage as the input features to detect ISCs. Our features only come from normal batteries and are better than conventional methods. Therefore, we can achieve faster and more accurate ISC detection.

Our methods provide a possibility for battery ISC detection using deep learning methods in real-life applications. The proposed method can also be extended to other fault detection tasks that may lead to abnormal voltage evolution, such as TRs, external short circuits, and lithium deposition, to achieve early detection and warning of various faults. The present study can be improved in the future. First, as a deep learning approach, the proposed method can be explored to apply to more dynamic and even practical working conditions to broaden its application scenarios. Second, in this work, only the dataset generated from NCM523 and NCM811 commercial batteries is used to evaluate the study. The proposed method can be explored to apply to more diverse battery types. Finally, accurate and robust ISC early detection methods for battery packs are also urgently needed in real life. We defer consideration of these aspects to future work.

EXPERIMENTAL PROCEDURES

Resource availability

Lead contact

Further information and requests for resources should be directed to and will be fulfilled by the lead contact, Chunyu Du (cydu@hit.edu.cn).

Materials availability

This study did not generate new unique materials.

Data and code availability

Data[52] generated during the study are available on Zenodo: https://doi.org/10.5281/zenodo.7703318. The code is available on GitHub: https://github.com/swhlqu/voltage_prediction_and_ISC_detection.

Deep learning method development

The developed voltage and power prediction model and ISC detection model based on deep learning approaches are depicted in Figure 6. In the developed voltage and power prediction model, the encoder and decoder inputs are first passed into the "positional encoding layer" and the one-dimensional (1D) convolutional layer for feature extraction. Then, we pass the encoder inputs, the second half of the encoder inputs, and the last quarter of encoder inputs into different networks, including the "encoder layer," "conv layer," and "layer normalization," which can reduce the computational complexity and increase the robustness and accuracy.[53] The "concat layer" concatenates the outputs from 3 paths. Afterward, the outputs from the "concat layer" and the results calculated by the "position encoding layer," the "input embedding layer," the "multi-head attention layer," and the "layer normalization" are passed together into the "multi-head attention layer" of the decoder. Following the "multi-head attention layer" are two 1D convolutional layers and "residual connections." The final layer is a dense layer whose size coincides with the length of the prediction target. The architecture of the ISC detection method is the same as the encoder part of the voltage and power prediction model up to the "concat layer." Afterward, a dense layer and a "flatten layer" transform the results' dimensions from the "concat layer." Finally, a dense layer whose soft version of max (softmax) is employed as the activation function yields the probability of ISCs. Detailed information on the proposed method is introduced in Note S3. The neural numbers and activation functions of each layer are listed in Table S15 and Note S3.

The proposed voltage and power prediction model and ISC detection method are trained by the Adam algorithm.[54] The batch size is 128, and the loss functions are the mean squared error (MSE) and cross-entropy.[55] An early stopping strategy[56] is adopted to prevent overfitting and enhance robustness. The proposed methods are trained for a maximum of 200 epochs, and the model with the minimum validation loss is selected as the final model.

RMSE and MAE are chosen to evaluate the performance of the voltage and power prediction model. RMSE and MAE are defined as

$$RMSE = \sqrt{\frac{1}{m}\sum_{i=1}^{m}(y_i - \hat{y}_i)^2} \quad \text{(Equation 1)}$$

$$MAE = \frac{1}{m}\sum_{i=1}^{m}|y_i - \hat{y}_i| \quad \text{(Equation 2)}$$

where y_i and $\hat{y}_i$ are the observed and predicted voltage sequences in the scenario of voltage prediction and the observed and predicted power sequences in the scenario of power prediction, respectively.

Average percentage accuracy is used to validate the ISC detection method performance. The average percentage accuracy is defined as

$$\%\ accuracy = \frac{TrueP + TrueN}{(TrueP + FalseP + TrueN + FalseN)} \quad \text{(Equation 3)}$$

where TrueP, TrueN, FalseP, and FalseN are the count of true positive, true negative, false positive, and false negative samples, respectively.[57]

Data processing and development of all proposed methods are implemented in Python 3.9 with Pytorch 1.11. The computation is executed based on an RTX 3090 graphics processing unit.

SUPPLEMENTAL INFORMATION

Supplemental information can be found online at https://doi.org/10.1016/j.patter.2023.100732.

ACKNOWLEDGMENTS

This work is supported by the Heilongjiang Touyan Innovation Team Program (HITTY-20190033).

AUTHOR CONTRIBUTIONS

Conceptualization, B.C. and C.D.; methodology, B.C., L.X., and H.Z.; software, B.C.; validation, B.C. and H.W.; formal analysis, B.C., H.Z., L.X., and R.L.; investigation, B.C. and H.W.; resources, B.C.; data curation, B.C., H.Z., L.X., and R.L.; writing – original draft, B.C., G.H., and C.D.; writing – review & editing, B.C., H.W., J.D., S.L., and X.Z.; visualization, B.C. and H.W.; supervision, C.D.; funding acquisition, C.D.

DECLARATION OF INTERESTS

The authors declare no competing interests.

Received: September 15, 2022
Revised: November 7, 2022
Accepted: March 24, 2023
Published: April 18, 2023

REFERENCES

1. Deng, J., Bae, C., Marcicki, J., Masias, A., and Miller, T. (2018). Safety modelling and testing of lithium-ion batteries in electrified vehicles. Nat. Energy *3*, 261–266. https://doi.org/10.1038/s41560-018-0122-3.
2. Liu, X., Ren, D., Hsu, H., Feng, X., Xu, G.-L., Zhuang, M., Gao, H., Lu, L., Han, X., Chu, Z., et al. (2018). Thermal runaway of lithium-ion batteries without internal short circuit. Joule *2*, 2047–2064. https://doi.org/10.1016/j.joule.2018.06.015.
3. Li, W., Zhu, J., Xia, Y., Gorji, M.B., and Wierzbicki, T. (2019). Data-driven safety envelope of lithium-ion batteries for electric vehicles. Joule *3*, 2703–2715. https://doi.org/10.1016/j.joule.2019.07.026.
4. Wang, S., Takyi-Aninakwa, P., Jin, S., Yu, C., Fernandez, C., and Stroe, D.-I. (2022). An improved feedforward-long short-term memory modeling method for the whole-life-cycle state of charge prediction of lithium-ion batteries considering current-voltage-temperature variation. Energy *254*, 124224. https://doi.org/10.1016/j.energy.2022.124224.
5. Wang, S., Jin, S., Bai, D., Fan, Y., Shi, H., and Fernandez, C. (2021). A critical review of improved deep learning methods for the remaining useful life prediction of lithium-ion batteries. Energy Rep. *7*, 5562–5574. https://doi.org/10.1016/j.egyr.2021.08.182.
6. Wang, Q., Ping, P., Zhao, X., Chu, G., Sun, J., and Chen, C. (2012). Thermal runaway caused fire and explosion of lithium ion battery. J. Power Sources *208*, 210–224. https://doi.org/10.1016/j.jpowsour.2012.02.038.
7. Huang, P., Ping, P., Li, K., Chen, H., Wang, Q., Wen, J., and Sun, J. (2016). Experimental and modeling analysis of thermal runaway propagation over the large format energy storage battery module with Li4Ti5O12 anode. Appl. Energy *183*, 659–673. https://doi.org/10.1016/j.apenergy.2016.08.160.
8. Larsson, F., Andersson, P., Blomqvist, P., and Mellander, B.E. (2017). Toxic fluoride gas emissions from lithium-ion battery fires. Sci. Rep. *7*, 10018. https://doi.org/10.1038/s41598-017-09784-z.
9. Ribière, P., Grugeon, S., Morcrette, M., Boyanov, S., Laruelle, S., and Marlair, G. (2012). Investigation on the fire-induced hazards of Li-ion

battery cells by fire calorimetry. Energy Environ. Sci. *5*, 5271–5280. https://doi.org/10.1039/c1ee02218k.

10. Feng, X., Ren, D., He, X., and Ouyang, M. (2020). Mitigating thermal runaway of lithium-ion batteries. Joule *4*, 743–770. https://doi.org/10.1016/j.joule.2020.02.010.

11. Kim, G.-H., Pesaran, A., and Spotnitz, R. (2007). A three-dimensional thermal abuse model for lithium-ion cells. J. Power Sources *170*, 476–489. https://doi.org/10.1016/j.jpowsour.2007.04.018.

12. Feng, X., Weng, C., Ouyang, M., and Sun, J. (2016). Online internal short circuit detection for a large format lithium ion battery. Appl. Energy *161*, 168–180. https://doi.org/10.1016/j.apenergy.2015.10.019.

13. Naha, A., Khandelwal, A., Hariharan, K.S., Kaushik, A., Yadu, A., and Kolake, S.M. (2019). On-board short-circuit detection of Li-ion batteries undergoing fixed charging profile as in smartphone applications. IEEE Trans. Ind. Electron. *66*, 8782–8791. https://doi.org/10.1109/tie.2018.2889623.

14. Naha, A., Khandelwal, A., Agarwal, S., Tagade, P., Hariharan, K.S., Kaushik, A., Yadu, A., Kolake, S.M., Han, S., and Oh, B. (2020). Internal short circuit detection in Li-ion batteries using supervised machine learning. Sci. Rep. *10*, 1301. https://doi.org/10.1038/s41598-020-58021-7.

15. Kang, Y., Duan, B., Zhou, Z., Shang, Y., and Zhang, C. (2020). Online multi-fault detection and diagnosis for battery packs in electric vehicles. Appl. Energy *259*, 114170. https://doi.org/10.1016/j.apenergy.2019.114170.

16. Zhang, Z., Kong, X., Zheng, Y., Zhou, L., and Lai, X. (2019). Real-time diagnosis of micro-short circuit for Li-ion batteries utilizing low-pass filters. Energy *166*, 1013–1024. https://doi.org/10.1016/j.energy.2018.10.160.

17. Xia, B., Shang, Y., Nguyen, T., and Mi, C. (2017). A correlation based fault detection method for short circuits in battery packs. J. Power Sources *337*, 1–10. https://doi.org/10.1016/j.jpowsour.2016.11.007.

18. Hong, J., Wang, Z., Chen, W., and Wang, L. (2019). Multi-fault synergistic diagnosis of battery systems based on the modified multi-scale entropy. Int. J. Energy Res. *43*, 8350–8369. https://doi.org/10.1002/er.4831.

19. Ma, M., Wang, Y., Duan, Q., Wu, T., Sun, J., and Wang, Q. (2018). Fault detection of the connection of lithium-ion power batteries in series for electric vehicles based on statistical analysis. Energy *164*, 745–756. https://doi.org/10.1016/j.energy.2018.09.047.

20. Ouyang, M., Zhang, M., Feng, X., Lu, L., Li, J., He, X., and Zheng, Y. (2015). Internal short circuit detection for battery pack using equivalent parameter and consistency method. J. Power Sources *294*, 272–283. https://doi.org/10.1016/j.jpowsour.2015.06.087.

21. Seo, M., Goh, T., Park, M., Koo, G., and Kim, S. (2017). Detection of internal short circuit in lithium ion battery using model-based switching model method. Energies *10*, 76. https://doi.org/10.3390/en10010076.

22. Seo, M., Goh, T., Park, M., and Kim, S. (2018). Detection method for soft internal short circuit in lithium-ion battery pack by extracting open circuit voltage of faulted cell. Energies *11*, 1669. https://doi.org/10.3390/en11071669.

23. Lai, X., Yi, W., Kong, X., Han, X., Zhou, L., Sun, T., and Zheng, Y. (2020). Online detection of early stage internal short circuits in series-connected lithium-ion battery packs based on state-of-charge correlation. J. Energy Storage *30*, 101514. https://doi.org/10.1016/j.est.2020.101514.

24. Zheng, Y., Gao, W., Ouyang, M., Lu, L., Zhou, L., and Han, X. (2018). State-of-charge inconsistency estimation of lithium-ion battery pack using mean-difference model and extended Kalman filter. J. Power Sources *383*, 50–58. https://doi.org/10.1016/j.jpowsour.2018.02.058.

25. Feng, X., Pan, Y., He, X., Wang, L., and Ouyang, M. (2018). Detecting the internal short circuit in large-format lithium-ion battery using model-based fault-diagnosis algorithm. J. Energy Storage *18*, 26–39. https://doi.org/10.1016/j.est.2018.04.020.

26. Kong, X., Zheng, Y., Ouyang, M., Lu, L., Li, J., and Zhang, Z. (2018). Fault diagnosis and quantitative analysis of micro-short circuits for lithium-ion batteries in battery packs. J. Power Sources *395*, 358–368. https://doi.org/10.1016/j.jpowsour.2018.05.097.

27. Zhang, G., Wei, X., Tang, X., Zhu, J., Chen, S., and Dai, H. (2021). Internal short circuit mechanisms, experimental approaches and detection methods of lithium-ion batteries for electric vehicles: a review. Renew. Sustain. Energy Rev. *141*, 110790. https://doi.org/10.1016/j.rser.2021.110790.

28. Hong, J., Wang, Z., and Yao, Y. (2019). Fault prognosis of battery system based on accurate voltage abnormity prognosis using long short-term memory neural networks. Appl. Energy *251*, 113381. https://doi.org/10.1016/j.apenergy.2019.113381.

29. Liu, Y., Liao, C., Zhang, W., Hu, G., Zhang, C., and Wang, L. (2022). Internal short circuit diagnosis of lithium-ion battery based on mechanism model and deep learning. J. Electrochem. Soc. *169*, 100514. https://doi.org/10.1149/1945-7111/ac91ab.

30. Cao, R., Zhang, Z., Lin, J., Lu, J., Zhang, L., Xiao, L., Liu, X., and Yang, S. (2022). Reliable online internal short circuit diagnosis on lithium-ion battery packs via voltage anomaly detection based on the mean-difference model and the adaptive prediction algorithm. Batteries *8*, 224. https://doi.org/10.3390/batteries8110224.

31. Hernandez, L., Baladron, C., Aguiar, J.M., Carro, B., Sanchez-Esguevillas, A.J., Lloret, J., and Massana, J. (2014). A survey on electric power demand forecasting: future trends in smart grids, microgrids and smart buildings. IEEE Commun. Surv. Tutorials *16*, 1460–1495. https://doi.org/10.1109/surv.2014.032014.00094.

32. Tian, S., Li, C., Lv, Q., and Li, J. (2022). Method for predicting the remaining mileage of electric vehicles based on dimension expansion and model fusion. IET Intelligent Trans. Sys. *16*, 1074–1091. https://doi.org/10.1049/itr2.12196.

33. Lai, X., Huang, Y., Gu, H., Han, X., Feng, X., Dai, H., Zheng, Y., and Ouyang, M. (2022). Remaining discharge energy estimation for lithium-ion batteries based on future load prediction considering temperature and ageing effects. Energy *238*, 121754. https://doi.org/10.1016/j.energy.2021.121754.

34. Mei, W., Jiang, L., Liang, C., Sun, J., and Wang, Q. (2021). Understanding of Li-plating on graphite electrode: detection, quantification and mechanism revelation. Energy Storage Mater. *41*, 209–221. https://doi.org/10.1016/j.ensm.2021.06.013.

35. Chen, Z., Xiong, R., Tian, J., Shang, X., and Lu, J. (2016). Model-based fault diagnosis approach on external short circuit of lithium-ion battery used in electric vehicles. Appl. Energy *184*, 365–374. https://doi.org/10.1016/j.apenergy.2016.10.026.

36. Zhao, R., Liu, J., and Gu, J. (2016). Simulation and experimental study on lithium ion battery short circuit. Appl. Energy *173*, 29–39. https://doi.org/10.1016/j.apenergy.2016.04.016.

37. Zheng, Y., Lu, Y., Gao, W., Han, X., Feng, X., and Ouyang, M. (2021). Micro-short-circuit cell fault identification method for lithium-ion battery packs based on mutual information. IEEE Trans. Ind. Electron. *68*, 4373–4381. https://doi.org/10.1109/tie.2020.2984441.

38. Zhou, H., Zhang, S., Peng, J., Zhang, S., Li, J., Xiong, H., and Zhang, W. (2021). Informer: beyond efficient transformer for long sequence time-series forecasting. AAAI. Conf. Artif. Intell *35*, 11106–11115. https://doi.org/10.48550/arXiv.2012.07436.

39. Cho, K., Merrienboer, B.v., Gulcehre, C., Bahdanau, D., Bougares, F., Schwenk, H., and Bengio, Y. (2014). Learning phrase representations using RNN encoder-decoder for statistical machine translation. Preprint at arXiv. https://doi.org/10.48550/arXiv.1406.1078.

40. Devlin, J., Chang, M.-W., Lee, K., and Toutanova, K. (2019). BERT: pre-training of deep bidirectional transformers for language understanding. Preprint at arXiv. https://doi.org/10.48550/arXiv.1810.04805.

41. Bloom, I., Christophersen, J.P., Abraham, D.P., and Gering, K.L. (2006). Differential voltage analyses of high-power lithium-ion cells. J. Power Sources *157*, 537–542. https://doi.org/10.1016/j.jpowsour.2005.07.054.

42. Smith, A.J., Burns, J.C., and Dahn, J.R. (2011). High-precision differential capacity analysis of LiMn2O4/graphite cells. Electrochem. Solid State Lett. *14*, A39–A41. https://doi.org/10.1149/1.3543569.

43. Dubarry, M., Truchot, C., and Liaw, B.Y. (2012). Synthesize battery degradation modes via a diagnostic and prognostic model. J. Power Sources *219*, 204–216. https://doi.org/10.1016/j.jpowsour.2012.07.016.

44. Berecibar, M., Devriendt, F., Dubarry, M., Villarreal, I., Omar, N., Verbeke, W., and Van Mierlo, J. (2016). Online state of health estimation on NMC cells based on predictive analytics. J. Power Sources *320*, 239–250. https://doi.org/10.1016/j.jpowsour.2016.04.109.

45. Anseán, D., Dubarry, M., Devie, A., Liaw, B.Y., García, V., Viera, J.C., and González, M. (2016). Fast charging technique for high power LiFePO4 batteries: a mechanistic analysis of aging. J. Power Sources *321*, 201–209. https://doi.org/10.1016/j.jpowsour.2016.04.140.

46. Anseán, D., Dubarry, M., Devie, A., Liaw, B.Y., García, V., Viera, J.C., and González, M. (2017). Operando lithium plating quantification and early detection of a commercial LiFePO4 cell cycled under dynamic driving schedule. J. Power Sources *356*, 36–46. https://doi.org/10.1016/j.jpowsour.2017.04.072.

47. Safari, M., and Delacourt, C. (2011). Simulation-based analysis of aging phenomena in a commercial graphite/LiFePO4 cell. J. Electrochem. Soc. *158*, A1436. https://doi.org/10.1149/2.103112jes.

48. Raj, T., Wang, A.A., Monroe, C.W., and Howey, D.A. (2020). Investigation of path-dependent degradation in lithium-ion batteries. Batter. Supercaps *3*, 1377–1385. https://doi.org/10.1002/batt.202000160.

49. Seo, M., Park, M., Song, Y., and Kim, S.W. (2020). Online detection of soft internal short circuit in lithium-ion batteries at various standard charging ranges. IEEE Access *8*, 70947–70959. https://doi.org/10.1109/access.2020.2987363.

50. Ma, M., Duan, Q., Li, X., Liu, J., Zhao, C., Sun, J., and Wang, Q. (2021). Fault diagnosis of external soft-short circuit for series connected lithium-ion battery pack based on modified dual extended Kalman filter. J. Energy Storage *41*, 102902. https://doi.org/10.1016/j.est.2021.102902.

51. Hu, J., Wei, Z., and He, H. (2021). An online adaptive internal short circuit detection method of lithium-ion battery. Automot. Innov. *4*, 93–102. https://doi.org/10.1007/s42154-020-00127-9.

52. Cui, B., Wang, H., Li, R., Xiang, L., Du, J., Zhao, H., Li, S., Zhao, X., Yin, G., Cheng, X., et al. (2023). Long-sequence voltage series forecasting for internal short circuit early detection of Lithium-ion batteries. Zenodo. https://doi.org/10.5281/zenodo.7703318.

53. Ashish, V., Noam, S., Niki, P., Jakob, U., Llion, J., Aidan, N.G., Lukasz, K., and Illia, P. (2017). Attention is all you need. Preprint at arXiv. https://doi.org/10.48550/arXiv.1706.03762.

54. Diederik, P.K., and Jimmy, L.B. (2015). Adam: a method for stochastic optimization. Preprint at arXiv. https://doi.org/10.48550/arXiv.1412.6980.

55. Zadeh, S.G., and Schmid, M. (2021). Bias in cross-entropy-based training of deep survival networks. IEEE Trans. Pattern Anal. Mach. Intell. *43*, 3126–3137. https://doi.org/10.1109/TPAMI.2020.2979450.

56. Tian, J., Xiong, R., Shen, W., and Lu, J. (2021). State-of-charge estimation of LiFePO4 batteries in electric vehicles: a deep-learning enabled approach. Appl. Energy *291*, 116812. https://doi.org/10.1016/j.apenergy.2021.116812.

57. Ibrahim, A.U., Ozsoz, M., Serte, S., Al-Turjman, F., and Yakoi, P.S. (2021). Pneumonia classification using deep learning from chest X-ray images during COVID-19. Cognit. Comput. 1–13. https://doi.org/10.1007/s12559-020-09787-5.